Geophysical Research Letters

RESEARCH LETTER
10.1029/2021GL095017

Diffusion-Free Scaling in Rotating Spherical Rayleigh-Bénard Convection

Guiquan Wang[1], Luca Santelli[2], Detlef Lohse[1,3], Roberto Verzicco[1,2,4], and Richard J. A. M. Stevens[1]

[1]Department of Science and Technology, Physics of Fluids Group and Twente Max Planck Center, Mesa+ Institute, J. M. Burgers Center for Fluid Dynamics, University of Twente, Enschede, The Netherlands, [2]Gran Sasso Science Institute, L'Aquila, Italy, [3]Max Planck Institute for Dynamics and Self-Organization, Göttingen, Germany, [4]Dipartimento di Ingegneria Industriale, University of Rome' Tor Vergata', Rome, Italy

Key Points:

- We show that in rotating spherical Rayleigh-Bénard convection, three regions with distinctly different flow dynamics are formed
- The mid-latitude region is characterized by convective columns that extend from the Northern to the Southern hemisphere of the outer sphere
- The diffusion-free scaling indicates that the flow dynamics and heat transport originating in the mid-latitude region are bulk-dominated

Supporting Information:

Supporting Information may be found in the online version of this article.

Correspondence to:

G. Wang and R. J. A. M. Stevens,
gwang4academy@gmail.com;
r.j.a.m.stevens@utwente.nl

Citation:

Wang, G., Santelli, L., Lohse, D., Verzicco, R., & Stevens, R. J. A. M. (2021). Diffusion-free scaling in rotating spherical Rayleigh-Bénard convection. *Geophysical Research Letters*, *48*, e2021GL095017. https://doi.org/10.1029/2021GL095017

Received 29 JUN 2021
Accepted 28 SEP 2021

Abstract Direct numerical simulations are employed to reveal three distinctly different flow regions in rotating spherical Rayleigh-Bénard convection. In the high-latitude region vertical (parallel to the axis of rotation) convective columns are generated between the hot inner and the cold outer sphere. The mid-latitude region II is dominated by vertically aligned convective columns formed between the Northern and Southern hemispheres of the outer sphere. The diffusion-free scaling, which indicates bulk-dominated convection, originates from this mid-latitude region. In the equator region III, the vortices are affected by the outer spherical boundary and are much shorter than in region II.

Plain Language Summary Thermally driven turbulence with background rotation in spherical Rayleigh-Bénard convection is found to be characterized by three distinctly different flow regions. The diffusion-free scaling, which indicates the heat transfer is bulk-dominated, originates from the mid-latitude region in which vertically aligned vortices are stretched between the Northern and Southern hemispheres of the outer sphere. These results show that the flow physics in rotating convection is qualitatively different in planar and spherical geometries. This finding underlines that it is crucial to study convection in spherical geometries to better understand geophysical and astrophysical flow phenomena.

1. Introduction

Rapidly rotating convection is relevant for many geophysical and astrophysical flows, e.g., the solar interior (Schumacher & Sreenivasan, 2020), the liquid metal core of terrestrial planets (Aurnou et al., 2015; Jones, 2011; Olson, 2011; Zhang & Schubert, 2000), and Earth's oceans and atmosphere (Fultz et al., 1959; Marshall & Schott, 1999). In these instances of convection with strong thermal driving, the flow dynamics is nevertheless dominated by the strong background rotation (Aurnou et al., 2015; Kunnen, 2021; Sprague et al., 2006). The effect of rotation has been extensively studied in Rayleigh-Bénard (RB) convection experiments (Cheng et al., 2020; Ecke & Niemela, 2014; King et al., 2009, 2012; Liu & Ecke, 1997; Rossby, 1969; Stellmach et al., 2014; Stevens et al., 2009; Wedi et al., 2021; Zhong et al., 2009) and simulations (Horn & Shishkina, 2015; King et al., 2012, 2013, 2009; Kunnen et al., 2016; Schmitz & Tilgner, 2009; Stellmach et al., 2014; Stevens et al., 2009). In the canonical RB system, the flow is confined between two parallel plates, and this system is studied in 3D periodic, rectangular, or cylindrical domains. In the remainder of this article, we refer to this as planar RB convection to distinguish it from the spherical RB system considered here (see Figure 1a). We refer the reader to the reviews (Aurnou et al., 2015; Kunnen, 2021; Plumley & Julien, 2019) for an extensive explanation of rotating RB convection. Even though there are great community efforts on rotating RB the diffusion-free scaling regime, geostrophic dominated which will be defined explicitly below, predicted for strongly thermally driven rotation dominated flow has not been observed yet for rotating RB with no-slip boundaries. This study will show that in a spherical RB convection, the geometry allows for the formation of a geostrophic dominated flow region that exhibits diffusion-free scaling in the mid-latitude region.

The control parameters of rotating RB flow are the Rayleigh (Ra), Ekman (Ek), and Prandtl (Pr) numbers, to be defined explicitly below. Derived from these, the convective Rossby number $Ro \equiv \sqrt{Ra/PrEk}/2$

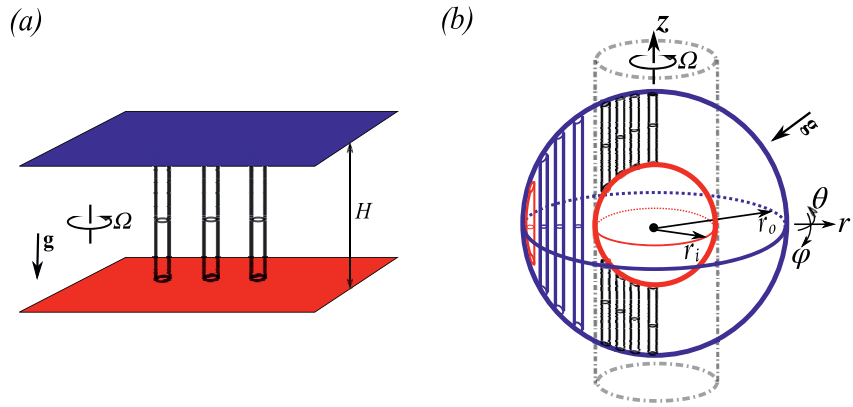

Figure 1. Schematics showing the alignment of the axial convective columns in (a) canonical framework heated from bottom and cooled from above and (b) spherical rotating RB convection heated from inner and cooled from outer, in which the gravity points toward the geometrical center. The longitudinal (azimuthal), co-latitudinal (polar), and radial directions are represented by $\hat{\theta}$, $\hat{\varphi}$ and $\hat{r}$, respectively. The rotation axis aligns with the z-direction. The angle between gravity and rotation axis is φ. The tangent cylinder is shown with dashed-dotted gray line. Panel (b) is adapted from Aurnou et al. (2015) and Busse (1970, 1983).

characterizes the importance of the thermal forcing relative to rotation (Gilman, 1977). With increasing Rayleigh number Ra and for strong rotation $Ro \ll 1$, two regimes can be identified, namely: (a) the *weakly nonlinear regime* for Ra near the onset of convection, (b) the *quasi-geostrophic regime* for $Ra/Ra_c \leq 3$ (Ecke & Niemela, 2014), where $Ra_c \sim Ek^{-4/3}$ is the critical Rayleigh number for the onset of convection (Chandrasekhar, 1961). In a third regime (c), for $Ro \gg 1$ and high enough Ra, the flow approaches the non-rotating RB convection case (Ahlers et al., 2009; Chilla & Schumacher, 2012; Grossmann & Lohse, 2000).

For the quasi-geostrophic regime, when $Ek \to 0$, the Nusselt number Nu (i.e., the non-dimensional heat transfer) is found to depend on the supercriticality $Nu \sim Pr^{\gamma}(Ra/Ra_c)^{\alpha}$ (Cheng et al., 2015; Julien, Knobloch, et al., 2012; King et al., 2012; Stellmach et al., 2014). When the heat transport is independent of molecular diffusion in the asymptotic limit, this results in $\alpha = 3/2$ and $\gamma = -1/2$. This scaling $Nu \sim Pr^{-1/2}(Ra/Ra_c)^{3/2}$ is known as *diffusion-free scaling*. The physics of the diffusion-free scaling, similar to the ultimate regime in RB convection (Grossmann & Lohse, 2011; Kraichnan, 1962; Shraiman & Siggia, 1990; Spiegel, 1971), is that the thermal and kinetic boundary layers, and thus the kinematic viscosity and thermal diffusivity, do not play an explicit role anymore for the heat flux scaling. This is known as bulk-dominated convection.

So far, the diffusion-free scaling has only been obtained in planar convection by considering an asymptotically reduced model in which Ekman pumping effects are not represented (Julien, Knobloch, et al., 2012) and numerical simulation with free-stress boundaries and $Ek \leq 10^{-6}$ (Kunnen et al., 2016; Stellmach et al., 2014). For planar convection with no-slip boundaries, King et al. (2012, 2013) theoretically predict $\alpha = 3$ for $Ra \lesssim Ek^{-3/2}$. This finding follows from an analysis of the boundary layer stability and is supported by experimental and simulation data for $10^{-6} \leq Ek \leq \infty$. The difference between $\alpha = 3$ for no-slip boundaries and $\alpha = 3/2$ for free-stress boundaries is attributed to the active role of the Ekman pumping in the boundary layers near the plates (Julien et al., 2016; Plumley et al., 2016). However, the asymptotic diffusion-free scaling exponent $\alpha = 3/2$ has not been reported for no-slip boundaries in planar convection.

However, Gastine et al. (2016) find the diffusion-free scaling for $Ek \leq 10^{-5}$ for $6Ra_c \leq Ra \leq 0.4Ek^{-8/5}$ in spherical RB convection with inner-to-outer radius ratio $\eta = 0.6$ and no-slip boundaries. The $Ek^{-8/5}$ scaling is proposed by Julien, Knobloch, et al. (2012); Julien, Rubio, et al. (2012). We note that previous theories of Gilman (1977) (giving the transitional Rayleigh number $Ra_t \sim Ek^{-2}$ where Ra_t represents for the upper bound of the diffusion-free scaling region) and of King et al. (2009) (giving $Ra_t \sim Ek^{-7/4}$) do not appropriately capture the upper bound of the diffusion-free scaling region, which scales as $Ek^{-8/5}$.

The objective of this work is to elucidate the observation of diffusion-free scaling in spherical RB convection at relatively weak rotation ($Ek \sim 10^{-5}$), while this scaling is not observed in planar convection. For strong rotation $Ro \ll 1$, the Taylor Proudman effect (Taylor, 1923) favors invariance along the rotation axis. In

planar convection, see Figure 1a, the rotation axis is orthogonal to the plates, and the convective columns are homogeneously distributed in the horizontal direction and always stretch between the hot and cold plates. However, in spherical geometry, the rotation effect is latitude dependent; see Figure 1b, due to which three distinctly different flow regions are formed. Inside the inner sphere's tangent cylinder, the convective columns touch the inner and outer spherical boundaries. In the mid-latitude region, the convective columns are stretched between the Northern and Southern hemispheres of the outer sphere. Near the equator, the convective columns adjust themselves to the curved boundary. This work will show that the diffusion-free scaling originates from this mid-latitude region. The article is organized as follows: In Section 2, we introduce the rotating spherical RB system with its control parameters. Section 3 is an overview of our simulation results compared and validated to literature, subsequent analysis is performed in Sections 4 and 5. Finally, we conclude our findings in Section 6.

2. Numerical Method, Control and Response Parameters

A sketch of the rotating spherical RB geometry is shown in Figure 1b. A fluid fills a spherical shell between the inner sphere of radius r_i and outer sphere of radius r_o with distance $d = r_o - r_i$ from the inner one. The whole system rotates about the vertical z axis at angular velocity Ω. The surface temperature of the inner and outer spheres is kept constant at T_i, and T_o, respectively, with $T_i > T_o$. No-slip boundary conditions are imposed at both spheres. We solve the Navier-Stokes equations in spherical coordinates within the Boussinesq approximation, which in dimensionless form read:

$$\frac{\partial \mathbf{u}}{\partial t} + \mathbf{u}\cdot\nabla\mathbf{u} = -\nabla p + \sqrt{\frac{Pr}{Ra}}\nabla^2\mathbf{u} + gT\vec{e}_r - \frac{1}{Ro}\vec{e}_z\times\mathbf{u}\ ,\ \nabla\cdot\mathbf{u} = 0, \tag{1}$$

$$\frac{\partial T}{\partial t} + \mathbf{u}\cdot\nabla T = \frac{1}{\sqrt{RaPr}}\nabla^2 T. \tag{2}$$

where $\mathbf{u}(\vec{x},t)$, $p(\vec{x},t)$, $T(\vec{x},t)$, and $g(r)$ denote the fluid velocity, pressure, temperature and radially dependent gravitational acceleration.

In this study, we focus on a radius ratio $\eta = r_i/r_o = 0.6$ and the gravity profile $g(r) \sim (r_o/r)^2$ valid for homogeneous mass distribution to allow comparisons with non-rotating (Gastine et al., 2015) and rotating (Gastine et al., 2016) convection in spherical RB. This system configuration is considered representative for studying convection in gas giants (Long et al., 2020). Additionally, we perform simulations for $\eta = 0.35$ and $g(r) \sim (r_o/r)^{-1}$, which is considered an Earth-like configuration used by Long et al. (2020) and Yadav et al. (2016). The equations are discretized by a staggered central second-order finite-difference scheme in spherical coordinates (Santelli et al., 2020). We use a uniform grid in the longitudinal and co-latitudinal directions and ensure that the bulk and boundary layers are appropriately resolved (Stevens, Verzicco, & Lohse, 2010). The grid cells are clustered toward the inner and outer sphere to ensure the boundary layers are adequately resolved (Shishkina et al., 2010). Further details on the simulations are given in the Supporting Information S1.

The dynamics of rotating spherical RB convection are determined by the Rayleigh, Prandtl, and Ekman numbers:

$$Ra = \frac{\beta g_o d^3 \Delta T}{\kappa\nu},\ Pr = \frac{\nu}{\kappa},\ Ek = \frac{\nu}{\Omega d^2}, \tag{3}$$

where β is the thermal expansion coefficient, g_o is the gravity at the outer sphere, ν is the kinematic viscosity, and κ is the thermal diffusivity of the fluid. Ra is a measure of the thermal driving of the system, Ek characterizes the ratio of viscous to Coriolis forces, and Pr indicates the ratio of the viscous to thermal diffusivities. In this study we consider $Pr = 1$. We use the Rossby number $Ro \equiv \sqrt{Ra/Pr}\,Ek/2$ to evaluate the relative importance of rotation and buoyancy (Gilman, 1977). We normalize the results using the length scale $d = r_o - r_i$, the temperature difference ΔT between inner and outer sphere, and the free-fall velocity $U = \sqrt{\beta g_o \Delta T d}$.

The Nusselt number quantifies the non-dimensional heat transport:

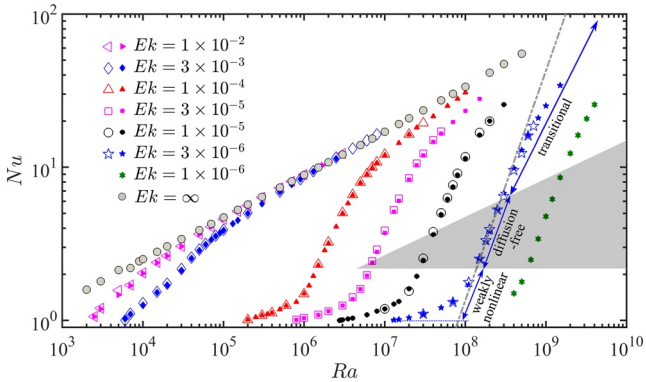

Figure 2. Nu as function of Ra for different Ek. Rotating cases: open symbols indicate the present results, filled-in symbols are those from Gastine et al. (2016). Non-rotating cases from Gastine et al. (2015) are indicated by $Ek = \infty$. The shaded wedge-shaped region indicates the diffusion-free scaling regime ($6Ek^{4/3} \le Ra \le 0.4Ek^{-8/5}$), which corresponds to the quasi-geostrophic regime identified by Gastine et al. (2016). The dot-dashed gray line gives the diffusion-free scaling $Nu = 0.149R^{3/2}$ for $Ek = 3 \times 10^{-6}$. The error bars are smaller than the symbol sizes.

$$Nu = \frac{\overline{\langle u_r T \rangle_s} - \kappa \partial_r \overline{\langle T \rangle_s}}{-\kappa \partial_r T_c}, \tag{4}$$

where $T_c(r) = \eta/[(1-\eta)^2 r] - \eta/(1-\eta)$ is the conductive temperature profile in spherical shells with constant temperature boundary conditions $T_c(r_i) = 1$ and $T_c(r_o) = 0$. The notations $\langle \cdots \rangle_s$ represents the average over a spherical surface with constant distance from the center, e.g., $\langle T \rangle_s = \frac{1}{4\pi}\int_0^{2\pi}\int_0^{\pi} T(\theta,r,\varphi)\sin\varphi \mathrm{d}\varphi \mathrm{d}\theta$. Overbar $\overline{\cdots}$ corresponds to time averaging. In the following discussion, we will use Nu on the outer sphere as a function of the co-latitude:

$$Nu(\varphi) = -\frac{1}{\eta}\frac{d\overline{\langle T \rangle_\theta}}{dr}\bigg|_{r_o} \tag{5}$$

where $\langle \ldots \rangle_\theta$ represents the average over the azimuthal direction, e.g., $\langle T \rangle_\theta = \frac{1}{2\pi}\int_0^{2\pi} T(\theta,r,\varphi)\mathrm{d}\theta$.

3. Heat Transfer in Rotating Spherical RB Convection

Figure 2 shows Nu as function of Ra for various Ek. The results from our simulations agree excellently with those from Gastine et al. (2016). For strong enough rotation (e.g., $Ek \le 3 \times 10^{-5}$), with increasing Ra three regimes can be identified (Gastine et al., 2016; Long et al., 2020). For low Ra, in the weakly nonlinear regime, rotational effects are dominant ($Ro \ll 1$) and $Nu \sim R^{\alpha}$ with $R \equiv RaEk^{4/3}$ and $\alpha = 1$. In the quasi-geostropic regime with diffusion-free scaling $\alpha = 3/2$, the Taylor-Proudman effect favors invariance along the rotation axis, thereby suppressing global heat transport relative to non-rotating case (Julien, Knobloch, et al., 2012). This regime is observed for $6Ek^{4/3} \le Ra \le 0.4Ek^{-8/5}$ (Gastine et al., 2016). The lower bound is related to Ra_c, while the upper bound corresponds to the asymptotic prediction for bulk-limited heat transfer in geostrophic turbulence by Julien, Knobloch, et al. (2012). In the transitional regime between strong and weak rotation ($Ro \sim 1$) the buoyancy force gradually becomes dominant over rotational effects with increasing Ra and the flow eventually approaches the non-rotating case for $Ro \gg 1$.

4. Identification of Three Flow Regimes

Figure 3a visualizes the columnar structures by $T' > 0$ and $T' < 0$, here $T'(\theta,r,\varphi) = T(\theta,r,\varphi) - \overline{\langle T \rangle_s}$, $\overline{\langle T \rangle_s}$ is defined in Section 2. The inner and outer thermal boundary layer thickness $\lambda_{T,i}$ and $\lambda_{T,o}$ is defined by the intersection of the linear fit to $\langle T \rangle_s$ near the boundaries and the profile at middepth (Gastine et al., 2016; Long et al., 2020). Figure 3b clearly shows that there are three distinct flow regions. Region I spans from the rotation axis to φ_1, where φ_1 can be determined by the intersection between the cylinder tangent to the inner sphere with the outer sphere. In this region, the columnar structures connect the boundary layers around the inner and outer spheres. Region II is found between φ_1 and φ_2 (see Figure 3b), φ_2 being the maximum zonal flow location (see below). In this mid-latitude region, the structures are the strongest, and tall thin columns stretch from the Northern to the Southern parts of the cold outer sphere. Region III is the region around the equator, see Figure 3b. In this region, the structures aligned with the rotation axis are much shorter than in the mid-latitude region II, while they conform themselves to the outer spherical boundary. Figure 3c shows that the heat transport strongly depends on the latitude (Yadav et al., 2016), which means that the heat transfer in the different flow regions identified above is different.

Aurnou and Olson (2001) and Christensen (2002) found that the zonal flow is prograde in the equatorial region near the outer boundary and retrogrades near the tangent cylinder that encloses the central core. Therefore, the zonal flow is suitable to identify the boundary between region II and III. Figures 4a and 4b show how we use the local maximum prograde zonal velocity close to the equator to set φ_2. Figure 4a

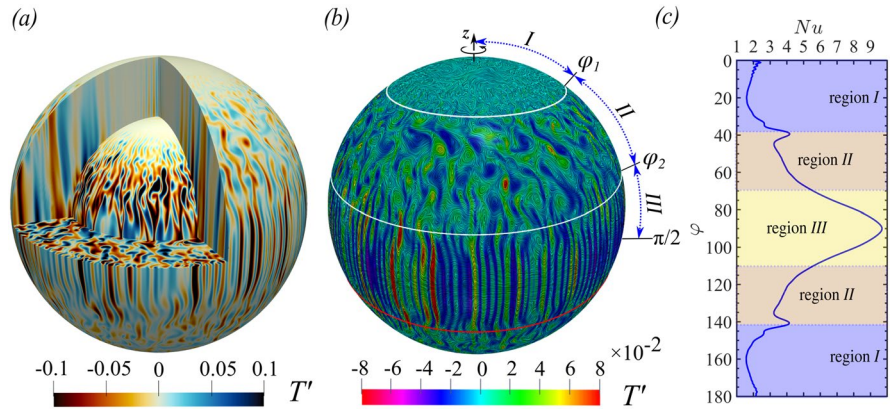

Figure 3. (a) Contour of the temperature fluctuation T' on two meridional cuts, equatorial section, and two spherical surfaces (corresponding to the spherical surfaces located at the inner ($r = r_i + \lambda_{T,i}$) and outer ($r = r_o - \lambda_{T,o}$) thermal boundary layers). (b) Contour of T' with streamlines illustrated by using line integral convolution on the outer radial surface (see Section 3 in the Supporting Information S1). The definition of the three regimes I, II, III is given in the text and Figure 4. (c) Nu as function of the co-latitude φ on the outer sphere. In all cases (a–c), $Ek = 1 \times 10^{-5}$ and $Ra = 5 \times 10^7$, i.e., simulation No.76 in the Supporting Information S1.

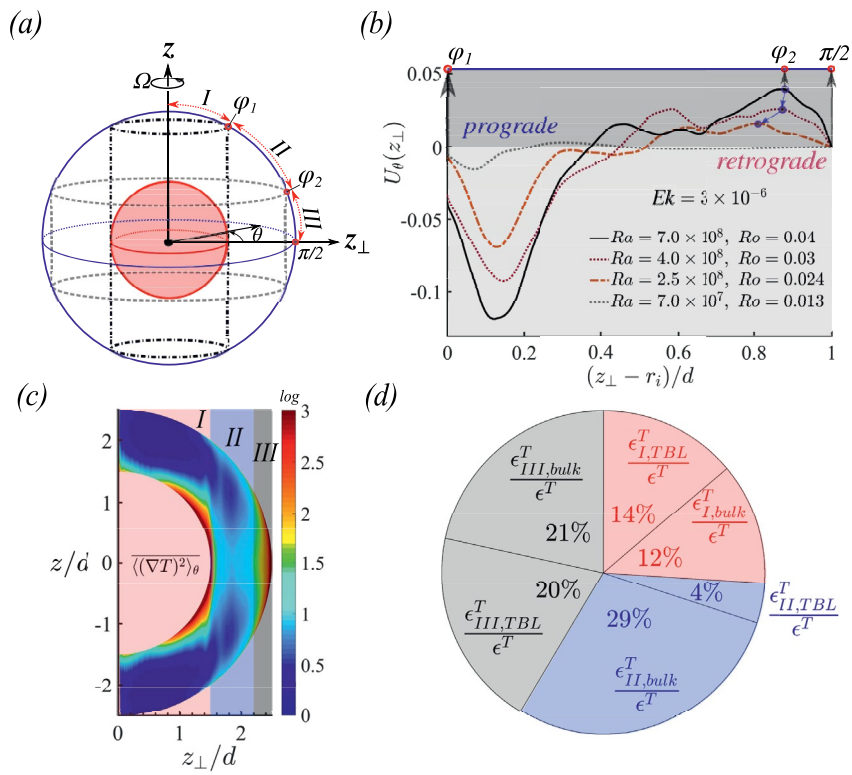

Figure 4. (a) Cylindrical polar coordinates $(z, z_\perp, \theta)$, z is the rotation axis, $z_\perp$ is the cylindrical radius and θ is the azimuthal angle and of which the regimes I, II, III can be defined as shown. (b) Ensemble averaged azimuthal velocities U_θ (zonal flows) as a function of $z_\perp$ in Equation 6. $(z_\perp - r_i)/d = 0$ and 1 correspond to the tangent cylinders of the inner and outer spheres, respectively. φ_2 is determined by the $z_\perp$ location close to the outer sphere ($(z_\perp - r_i)/d = 1$) where the zonal flow is strongest. (c) Time and azimuthal averaged thermal dissipation $\overline{\langle(\nabla T)^2\rangle_\theta}$ in the meridional plane for case No.76 of $Ek = 1 \times 10^{-5}$ and $Ra = 5 \times 10^7$. (d) Pie chart for (c) showing the distribution of the thermal dissipation rate over the different regions in the boundary layer and bulk, see Equation 8.

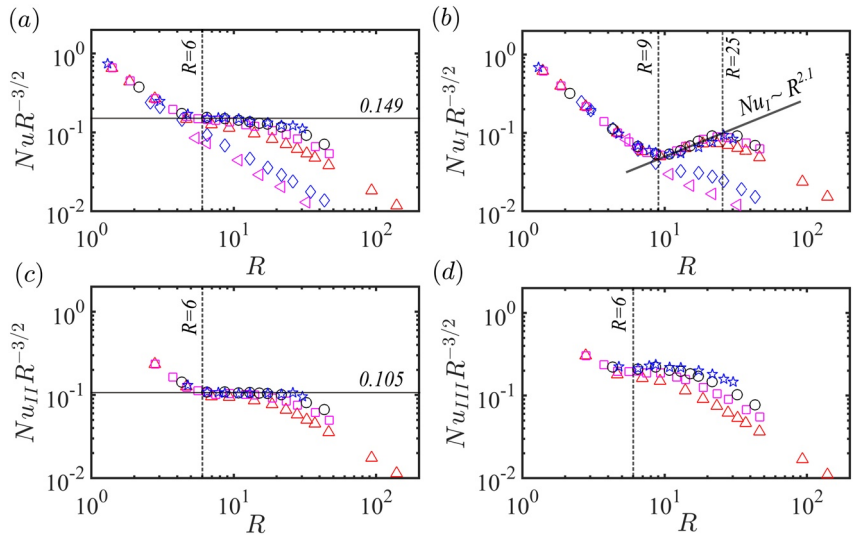

Figure 5. *Nu* on the outer sphere compensated by $R^{-3/2}$ and as a function of $R \equiv RaEk^{4/3}$. (a) Integration over the whole sphere; (b–d) *Nu* in regions (I – III), see Figure 3b. The symbols have the same meaning as in Figure 2.

illustrates the cylindrical coordinate system $(z, z_\perp, \theta)$ that is used to represent the zonal flow in Figure 4b. The zonal flow is the ensemble average of the azimuthal velocity in cylindrical coordinate:

$$U_\theta(z_\perp) = \overline{\langle u_\theta(z, z_\perp, \theta)\rangle_{\theta,z}} \tag{6}$$

where $u_\theta(z, z_\perp, \theta)$ is the longitudinal velocity $u_\theta(\theta, r, \phi)$ in spherical coordinate projected to cylindrical coordinate, $\langle\cdots\rangle_{\theta,z}$ indicates spatial average over a cylindrical surface (in the azimuthal and vertical direction), and $\overline{\cdots}$ indicates time-averaging.

We analyze the thermal dissipation in the different flow regions to determine whether the different regions are dominated by the boundary layer or the bulk dynamics. For spherical shells with radius ratio η, the thermal dissipation rate:

$$\epsilon^T \equiv \overline{\langle(\nabla T)^2\rangle} = \frac{3\eta}{1+\eta+\eta^2} Nu \tag{7}$$

by volume integral of $T \times (2)$. Figure 4c shows the time-averaged thermal dissipation rate in the meridional plane. The figure shows that the thermal dissipation intensity is highest in the boundary layers along the inner sphere (region I) and close to the equator region along the outer sphere (region III). We determine the distribution of the thermal dissipation rate over the different regions as follows:

$$\epsilon^T = \epsilon^T_{I,bulk} + \epsilon^T_{I,TBL} + \epsilon^T_{II,bulk} + \epsilon^T_{II,TBL} + \epsilon^T_{III,bulk} + \epsilon^T_{III,TBL,} \tag{8}$$

where bulk indicates the bulk regions and TBL indicates the thermal boundary layer regions, i.e., for the radial locations r; $r_i \le r \le r_i + \lambda_{T,i}$ along the inner sphere and $r_o - \lambda_{T,o} \le r \le r_o$ along the outer sphere. Figure 4d confirms that regions I and III are both strongly affected by the boundary layer dynamics. However, region II turns out to be bulk-dominated. We note that the boundary between region II and III is not determined based on the thermal dissipation profiles as there is not a clear peak in the direction separating the regimes. Therefore, as discussed above, we use the maximum in the zonal flow profile to determine this transition.

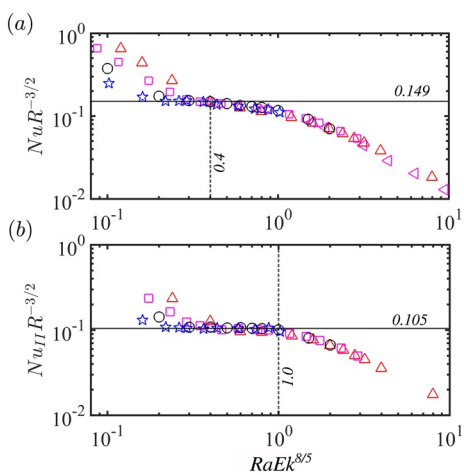

Figure 6. *Nu* compensated by $R^{-3/2}$ as a function of $RaEk^{8/5}$. (a) Integration over the whole sphere. The horizontal line is $NuR^{-3/2} = 0.149$ and the vertical line is $RaEk^{8/5} = 0.4$; (b) Region II. The horizontal line is $NuR^{-3/2} = 0.105$ and the vertical line is $RaEk^{8/5} = 1$. The symbols have the same meaning as in Figure 2.

In the following section, we will show that, in agreement with theoretical expectations discussed above, the scaling of the heat transfer in the region II follows the diffusion-free scaling for rotation dominated strongly thermally driven flows.

5. Diffusion-Free Scaling in Region II

Figure 5 shows Nu on the outer sphere compensated with the diffusion-free scaling law. Panel 5(a) shows that for the global heat transfer and $Ek \leq 5 \times 10^{-5}$ the diffusion-free scaling is observed for $R \geq 6$. The cross-over from the quasi-geostrophic region to the transitional region is observed at $Ra_t = 0.4Ek^{-8/5}$ (Gastine et al., 2016). Figures 5b–5d show the heat transfer scaling in the different flow regions identified above. Panel 5(b) evidences that, due to Ekman pumping (Stellmach et al., 2014; Stevens, Clercx, & Lohse, 2010; Stevens et al., 2013; Zhong et al., 2009), the heat transport scaling in region I is $Nu_{\mathrm{I}} \sim R^{2.1}$. This is steeper than the $\alpha = 3/2$ scaling for diffusion-free convection, but shallower than the $\alpha = 3$ value observed in planar convection (King et al., 2013). Most importantly, panel 5(c) shows that the diffusion-free scaling is much more pronounced in region II than in region I. Although the diffusion-free scaling still starts at $R = 6$, it continues for much higher R than the global heat transfer, see Figure 5a. Panel 5(d) shows that no diffusion-free scaling regime is observed in region III.

The diffusion-free scaling regime is observed from $6R$ up to Ra_t, where Ra_t indicates the Ra number at which the regime for bulk-limited heat transfer in geostrophic turbulence ends (Julien, Knobloch, et al., 2012; Julien, Rubio, et al., 2012). It was demonstrated (Gastine et al., 2016) that for the global heat transfer the diffusion-free scaling regime is observed up to $Ra_t = 0.4Ek^{-8/5}$, see also Figure 6a. For region II, Figure 6b shows that the diffusion-free scaling is observed up to $Ra_t = Ek^{-8/5}$, which is considerably higher Ra than for the global heat transport.

In Section 4 of the Supporting Information S1, we show that the observation of the diffusion-free scaling in the mid-latitude region II does not depend on the specific $\eta = 0.6$, $g(r) \sim (r_o/r)^2$ considered here. The same conclusion is obtained by analyzing $\eta = 0.35$, $g(r) \sim (r_o/r)^{-1}$ and $Ek = 1 \times 10^{-5}$.

6. Conclusions

In conclusion, we have shown that rotating spherical RB convection has three distinctly different flow regions; see Figure 3b. In region I, convective columns are formed between the hot inner and cold outer spheres. The mid-latitude region II is the region where the vertically aligned vortices are strongest, and the flow is bulk dominated. Region III is formed around the equator, and here the vortices are shorter and are affected by the outer spherical boundary.

The diffusion-free scaling $Nu \sim (RaEk^{4/3})^{\alpha}$ with $\alpha = 3/2$ originates from the mid-latitude flow region in which the flow dynamics are bulk dominated. In this region, thin and long convective columns are formed between the Northern and Southern parts of the cold outer sphere. This geostrophically dominated flow region can be formed due to the system geometry. Due to the curvature effects in spherical geometries, the latitude-dependent Coriolis force results in inhomogeneous convective columns in the co-latitudinal direction and more convective columns on the outer sphere than the inner sphere.

Acknowledgments
The authors thank the two anonymous referees for constructive comments that improved the manuscript. G. W. thanks Dr. Kai Leong Chong and Dr. Chong Shen Ng for insightful discussions. G. W. and R. J. A. M. S. acknowledge the financial support from ERC (the European Research Council) Starting Grant No. 804283 UltimateRB. This work was sponsored by NWO Science for the use of supercomputer facilities. The authors also acknowledge the national e-infrastructure of SURFsara, a subsidiary of SURF cooperation, the collaborative ICT organization for Dutch education and research, and Irene at Très Grand Centre de Calcul du CEA (TGCC) under PRACE project 2019215098. We acknowledge PRACE for awarding us access to MareNostrum at Barcelona Supercomputing Center (BSC), Spain (Project 2020235589, 2020225335).

Data Availability Statement

The data used in this article are available for download at https://doi.org/10.5281/zenodo.5034407.

References

Ahlers, G., Grossmann, S., & Lohse, D. (2009). Heat transfer and large scale dynamics in turbulent Rayleigh-Bénard convection. *Reviews of Modern Physics*, *81*, 503–537. https://doi.org/10.1103/revmodphys.81.503

Aurnou, J. M., Calkins, M. A., Cheng, J. S., Julien, K., King, E. M., Nieves, D., et al. (2015). Rotating convective turbulence in Earth and planetary cores. *Physics of the Earth and Planetary Interiors*, *246*, 52–71. https://doi.org/10.1016/j.pepi.2015.07.001

Aurnou, J. M., & Olson, P. L. (2001). Strong zonal winds from thermal convection in a rotating spherical shell. *Geophysical Research Letters*, *28*(13), 2557–2559. https://doi.org/10.1029/2000gl012474

Busse, F. H. (1970). Thermal instabilities in rapidly rotating systems. *Journal of Fluid Mechanics*, *44*(3), 441–460. https://doi.org/10.1017/s0022112070001921

Busse, F. H. (1983). A model of mean zonal flows in the major planets. *Geophysical & Astrophysical Fluid Dynamics*, *23*(2), 153–174. https://doi.org/10.1080/03091928308221746

Chandrasekhar, S. (1961). *Hydrodynamic and hydrodynamic stability*. Oxford University Press.

Cheng, J. S., Madonia, M., Aguirre Guzmán, A. J., & Kunnen, R. P. J. (2020). Laboratory exploration of heat transfer regimes in rapidly rotating turbulent convection. *Physical Review Fluids*, *5*, 113501. https://doi.org/10.1103/physrevfluids.5.113501

Cheng, J. S., Stellmach, S., Ribeiro, A., Grannan, A., King, E. M., & Aurnou, J. M. (2015). Laboratory-numerical models of rapidly rotating convection in planetary cores. *Geophysical Journal International*, *201*(1), 1–17. https://doi.org/10.1093/gji/ggu480

Chilla, F., & Schumacher, J. (2012). New perspectives in turbulent Rayleigh-Bénard convection. *The European Physical Journal E*, *35*, 58. https://doi.org/10.1140/epje/i2012-12058-1

Christensen, U. R. (2002). Zonal flow driven by strongly supercritical convection in rotating spherical shells. *Journal of Fluid Mechanics*, *470*, 115–133. https://doi.org/10.1017/s0022112002002008

Ecke, R. E., & Niemela, J. J. (2014). Heat transport in the geostrophic regime of rotating Rayleigh-Bénard convection. *Physical Review Letters*, *113*(11), 114301. https://doi.org/10.1103/physrevlett.113.114301

Fultz, D., Long, R. R., Owens, G. V., Bohan, W., Kaylor, R., & Weil, J. (1959). Studies of thermal convection in a rotating cylinder with some implications for large-scale atmospheric motions. *Studies of thermal convection in a rotating cylinder with some implications for large-scale atmospheric motions* (pp. 1–104). Springer. https://doi.org/10.1007/978-1-940033-37-2_1

Gastine, T., Wicht, J., & Aurnou, J. M. (2015). Turbulent Rayleigh-Bénard convection in spherical shells. *Journal of Fluid Mechanics*, *778*, 721–764. https://doi.org/10.1017/jfm.2015.401

Gastine, T., Wicht, J., & Aurnou, J. M. (2016). Scaling regimes in spherical shell rotating convection. *Journal of Fluid Mechanics*, *808*, 690–732. https://doi.org/10.1017/jfm.2016.659

Gilman, P. A. (1977). Nonlinear dynamics of Boussinesq convection in a deep rotating spherical shell-I. *Geophysical & Astrophysical Fluid Dynamics*, *8*(1), 93–135. https://doi.org/10.1080/03091927708240373

Grossmann, S., & Lohse, D. (2000). Scaling in thermal convection: A unifying theory. *Journal of Fluid Mechanics*, *407*, 27–56. https://doi.org/10.1017/s0022112099007545

Grossmann, S., & Lohse, D. (2011). Multiple scaling in the ultimate regime of thermal convection. *Physics of Fluids*, *23*(4), 045108. https://doi.org/10.1063/1.3582362

Horn, S., & Shishkina, O. (2015). Toroidal and poloidal energy in rotating Rayleigh-Bénard convection. *Journal of Fluid Mechanics*, *762*, 232–255. https://doi.org/10.1017/jfm.2014.652

Jones, C. A. (2011). Planetary magnetic fields and fluid dynamos. *Annual Review of Fluid Mechanics*, *43*, 583–614. https://doi.org/10.1146/annurev-fluid-122109-160727

Julien, K., Aurnou, J. M., Calkins, M. A., Knobloch, E., Marti, P., Stellmach, S., & Vasil, G. M. (2016). A nonlinear model for rotationally constrained convection with Ekman pumping. *Journal of Fluid Mechanics*, *798*, 50–87. https://doi.org/10.1017/jfm.2016.225

Julien, K., Knobloch, E., Rubio, A. M., & Vasil, G. M. (2012). Heat transport in low-Rossby-number Rayleigh-Bénard convection. *Physical Review Letters*, *109*(25),254503. https://doi.org/10.1103/physrevlett.109.254503

Julien, K., Rubio, A. M., Grooms, I., & Knobloch, E. (2012). Statistical and physical balances in low Rossby number Rayleigh-Bénard convection. *Geophysical & Astrophysical Fluid Dynamics*, *106*(4–5), 392–428. https://doi.org/10.1080/03091929.2012.696109

King, E. M., Stellmach, S., & Aurnou, J. M. (2012). Heat transfer by rapidly rotating Rayleigh-Bénard convection. *Journal of Fluid Mechanics*, *691*, 568–582. https://doi.org/10.1017/jfm.2011.493

King, E. M., Stellmach, S., & Buffett, B. (2013). Scaling behaviour in Rayleigh-Bénard convection with and without rotation. *Journal of Fluid Mechanics*, *717*, 449–471. https://doi.org/10.1017/jfm.2012.586

King, E. M., Stellmach, S., Noir, J., Hansen, U., & Aurnou, J. M. (2009). Boundary layer control of rotating convection systems. *Nature*, *457*(7227), 301–304. https://doi.org/10.1038/nature07647

Kraichnan, R. H. (1962). Turbulent thermal convection at arbitrary Prandtl number. *Physics of Fluids*, *5*(11), 1374–1389. https://doi.org/10.1063/1.1706533

Kunnen, R. P. J. (2021). The geostrophic regime of rapidly rotating turbulent convection. *Journal of Turbulence*, *22*(4–5), 267–296. https://doi.org/10.1080/14685248.2021.1876877

Kunnen, R. P. J., Ostilla-Mónico, R., Van Der Poel, E. P., Verzicco, R., & Lohse, D. (2016). Transition to geostrophic convection: The role of the boundary conditions. *Journal of Fluid Mechanics*, *799*, 413–432. https://doi.org/10.1017/jfm.2016.394

Liu, Y., & Ecke, R. E. (1997). Heat transport scaling in turbulent Rayleigh-Bénard convection: Effects of rotation and Prandtl number. *Physical Review Letters*, *79*(12), 2257–2260. https://doi.org/10.1103/physrevlett.79.2257

Long, R. S., Mound, J. E., Davies, C. J., & Tobias, S. M. (2020). Scaling behaviour in spherical shell rotating convection with fixed-flux thermal boundary conditions. *Journal of Fluid Mechanics*, *889*, A7. https://doi.org/10.1017/jfm.2020.67

Marshall, J., & Schott, F. (1999). Open-ocean convection: Observations, theory, and models. *Reviews of Geophysics*, *37*(1), 1–64. https://doi.org/10.1029/98rg02739

Olson, P. (2011). Laboratory experiments on the dynamics of the core. *Physics of the Earth and Planetary Interiors*, *187*(3–4), 139–156. https://doi.org/10.1016/j.pepi.2011.08.006

Plumley, M., & Julien, K. (2019). Scaling laws in Rayleigh-Bénard convection. *Earth and Space Science*, *6*(9), 1580–1592. https://doi.org/10.1029/2019ea000583

Plumley, M., Julien, K., Marti, P., & Stellmach, S. (2016). The effects of Ekman pumping on quasi-geostrophic Rayleigh-Bénard convection. *Journal of Fluid Mechanics*, *803*, 51–71. https://doi.org/10.1017/jfm.2016.452

Rossby, H. (1969). A study of Bénard convection with and without rotation. *Journal of Fluid Mechanics*, *36*(2), 309–335. https://doi.org/10.1017/s0022112069001674

Santelli, L., Orlandi, P., & Verzicco, R. (2020). A finite-difference scheme for three-dimensional incompressible flows in spherical coordinates. *Journal of Computational Physics*, *424*, 109848. https://doi.org/10.1016/j.jcp.2020.109848

Schmitz, S., & Tilgner, A. (2009). Heat transport in rotating convection without Ekman layers. *Physical Review E*, *80*(1), 015305. https://doi.org/10.1103/physreve.80.015305

Schumacher, J., & Sreenivasan, K. R. (2020). Colloquium: Unusual dynamics of convection in the Sun. *Reviews of Modern Physics*, *92*(4), 041001. https://doi.org/10.1103/revmodphys.92.041001

Shishkina, O., Stevens, R. J. A. M., Grossmann, S., & Lohse, D. (2010). Boundary layer structure in turbulent thermal convection and its consequences for the required numerical resolution. *New Journal of Physics*, *12*(7), 075022. https://doi.org/10.1088/1367-2630/12/7/075022

Shraiman, B. I., & Siggia, E. D. (1990). Heat transport in high-Rayleigh-number convection. *Physical Review A*, *42*(6), 3650–3653. https://doi.org/10.1103/physreva.42.3650

Spiegel, E. A. (1971). Convection in stars I. Basic Boussinesq convection. *Annual Review of Astronomy and Astrophysics*, *9*(1), 323–352. https://doi.org/10.1146/annurev.aa.09.090171.001543

Sprague, M., Julien, K., Knobloch, E., & Werne, J. (2006). Numerical simulation of an asymptotically reduced system for rotationally constrained convection. *Journal of Fluid Mechanics*, *551*, 141. https://doi.org/10.1017/s0022112005008499

Stellmach, S., Lischper, M., Julien, K., Vasil, G., Cheng, J. S., Ribeiro, A., et al. (2014). Approaching the asymptotic regime of rapidly rotating convection: Boundary layers versus interior dynamics. *Physical Review Letters*, *113*(25), 254501. https://doi.org/10.1103/physrevlett.113.254501

Stevens, R. J. A. M., Clercx, H. J. H., & Lohse, D. (2010). Optimal Prandtl number for heat transfer in rotating Rayleigh-Bénard convection. *New Journal of Physics*, *12*(7), 075005. https://doi.org/10.1088/1367-2630/12/7/075005

Stevens, R. J. A. M., Clercx, H. J. H., & Lohse, D. (2013). Heat transport and flow structure in rotating Rayleigh-Bénard convection. *European Journal of Mechanics - B/Fluids*, *40*, 41–49. https://doi.org/10.1016/j.euromechflu.2013.01.004

Stevens, R. J. A. M., Verzicco, R., & Lohse, D. (2010). Radial boundary layer structure and Nusselt number in Rayleigh-Bénard convection. *Journal of Fluid Mechanics*, *643*, 495–507. https://doi.org/10.1017/s0022112009992461

Stevens, R. J. A. M., Zhong, J.-Q., Clercx, H. J., Ahlers, G., & Lohse, D. (2009). Transitions between turbulent states in rotating Rayleigh-Bénard convection. *Physical Review Letters*, *103*(2), 024503. https://doi.org/10.1103/physrevlett.103.024503

Taylor, G. I. (1923). VIII. Stability of a viscous liquid contained between two rotating cylinders. *Philosophical Transactions of the Royal Society of London. Series A*, *223*(605–615), 289–343. https://doi.org/10.1098/rsta.1923.0008

Wedi, M., Gils, D. P. M. V., Bodenschatz, E., & Weiss, S. (2021). Rotating turbulent thermal convection at very large Rayleigh numbers. *Journal of Fluid Mechanics*, *912*, A30. https://doi.org/10.1017/jfm.2020.1149

Yadav, R. K., Gastine, T., Christensen, U. R., Duarte, L., & Reiners, A. (2016). Effect of shear and magnetic field on the heat-transfer efficiency of convection in rotating spherical shells. *Geophysical Journal International*, *204*(2), 1120–1133. https://doi.org/10.1093/gji/ggv506

Zhang, K., & Schubert, G. (2000). Magnetohydrodynamics in rapidly rotating spherical systems. *Annual Review of Fluid Mechanics*, *32*(1), 409–443. https://doi.org/10.1146/annurev.fluid.32.1.409

Zhong, J.-Q., Stevens, R. J. A. M., Clercx, H. J., Verzicco, R., Lohse, D., & Ahlers, G. (2009). Prandtl-, Rayleigh-, and Rossby-number dependence of heat transport in turbulent rotating Rayleigh-Bénard convection. *Physical Review Letters*, *102*(4), 044502. https://doi.org/10.1103/physrevlett.102.044502

References From the Supporting Information

Al-Shamali, F. M., Heimpel, M. H., & Aurnou, J. M. (2004). Varying the spherical shell geometry in rotating thermal convection. *Geophysical & Astrophysical Fluid Dynamics*, *98*(2), 153–169.

Cabral, B., & Leedom, L. C. (1993). Imaging vector fields using line integral convolution. *Proceedings of the 20th annual conference on computer graphics and interactive techniques* (pp. 263–270).

Hege, H. C., & Polthier, K. (2013). *Visualization and mathematics iii*. Springer Science & Business Media.